RSC Advances

ROYAL SOCIETY OF CHEMISTRY

www.rsc.org/advances

Journal Name

ARTICLE

The synthesis of 3D InN architectures via chemical vapor deposition and their optical properties†

Received 00th January 20xx,
Accepted 00th January 20xx

DOI: 10.1039/x0xx00000x

www.rsc.org/

Yunxuan Dong,[a] Shunxi Tang,[b] Hang Cui,*[a] Jian Zhang[a] and Qiliang Cui[a]

Indium nitride (InN) nanostructure is critical for the fabrication of optoelectronic and electronic devices. Up to now, great progress has been achieved in controlled synthesis of the low-dimensional nanostructures such as nanowires. However, the growth of the self-organized of uniform nanowires into well-defined three-dimensional (3D) superstructures has been rarely reported. Herein, two kinds of 3D InN microstructures which were synthesized by using chemical vapor deposition (CVD) was studied in detail to understand the growth mechanisms involved with the so-called "self-organized" schemes. The observations suggest that the formation of the InN microsphere and the split octahedron-like microstructure could be attributed to the different self-organized processes. However, the growth mechanisms of the 3D InN microstructures are substantially different from previous reports. The photoluminescence (PL) spectra of the InN microstructures recorded under room temperature condition with a broad photoluminescence emission band can be clearly observed in the spectrum range of 540 to 800 nm, which strongly suggest that the obtained microstructures is a direct semiconductor which exhibit a band gap of ~2.17 eV. Thus, it is anticipated that controlling the growth processes may be a potential route to tailor the morphology, microstructure, and even the properties of materials.

Introduction

Semiconductors in III-V groups, especially the nitrides, have become extremely important technological materials over the past decade due to the large direct band gap range and high thermal conductivity as well as high hardness, which makes them suitable for the fabrication of optoelectronic and electronic devices.[1-5] In particular, among the III-nitride compounds, InN has drawn substantial attention for the structures and physical properties under different conditions by reason of the smallest electron effective mass and direct band gap, the largest mobility, the highest peak and saturation electron drift velocities.[6,7] However, the large-scale growth of InN nanostructures still stays in immature stage due to the difficulties associated with extremely high equilibrium vapor pressure of indium and nitrogen and the low dissociation temperature of InN.[8-10]

On this regard, many efforts have been made for fabricating different InN nanostructures and investigating the crystal growth mechanisms. Great progress has been achieved in synthetic strategies, controlled synthesis of the primary building blocks such as nanoparticles, nanowires,[11,12] nanobelts,[13] and nanorods.[14,15] InN nanostructures have been prepared by several routes including atomic layer epitaxy (ALE), molecular beam epitaxy (MBE), chemical beam epitaxy (CBE), and chemical vapor deposition (CVD), etc..[15-20] Among these methods, the CVD without catalyst-assisted method is simple, effective and inexpensive for large-scale production. However, compared with other III-nitride compounds, the growth of 3D InN nanostructures, especially the self-organized of uniform primary building blocks into well-defined 3D superstructures, remains unclear. Recently, the self-organized of nanoparticles and subsequent formation of well-defined nanostructures has attracted rapidly growing interest owing to the important applications in nanoelectronics, magnetics, optoelectronics, photonics, heterogeneous catalysis, and so forth.[21] More importantly, this study provides the opportunity to explore the collective properties of assemblies of particles.[22,23]

In this work, two well-defined 3D InN microstructures were synthesized via a simple CVD without catalyst-assist. Detailed characterizations of morphology, structure and composition of the sample were performed. The self-organized process and the potential growth mechanism were discussed. The optical properties of the as-obtained 3D architectures were investigated as well.

Experimental

The InN microstructures were prepared via a CVD method.[24,25] Ultrasonically cleaned Si(100) wafers, without hydrofluoric acid etching, in size of 1 cm long and 1 cm wide, were applied as substrates for InN microstructure deposition. The starting materials of 0.1 g In powders in high purity (99.99%) were placed uniformly in

[a] State Key Laboratory of Superhard Materials and College of Physics, Jilin University, Changchun, 130012, China E-mail: cuihang@jlu.edu.cn
[b] School of Computer, Jiangxi University of Traditional Chinese Medicine, Nanchang, Jiangxi 330004, China

† Electronic supplementary information (ESI) available.

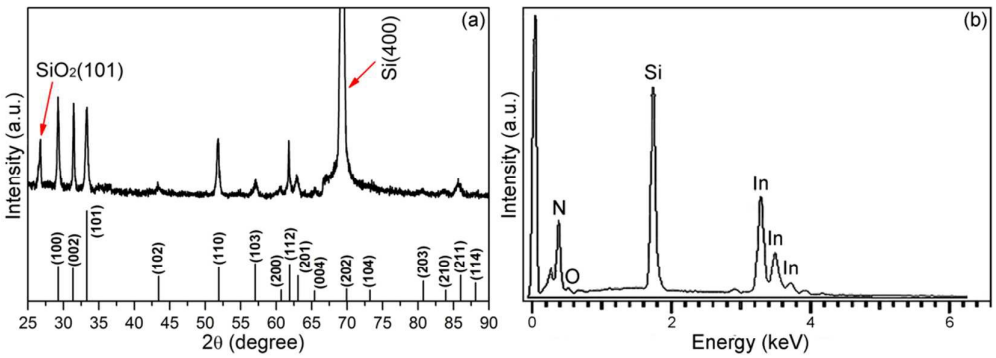

Fig. 1 (a) The typical XRD pattern of the as prepared InN sample. (b) The corresponding EDS spectra of the InN sample.

the quartz boat. The cleaned substrate was placed face down on the quartz boat. Then, the quartz boat was loaded at the center of a quartz tube, which was placed in a horizontal tube furnace. The quartz tube was degassed and then purged with high purity (99.999%) nitrogen for several times. High purity (99.999%) ammonia was employed as the reactive nitrogen source. After removing O_2 and H_2O by evacuating and nitrogen flushing for several times, the furnace was heated up under the protective flow of nitrogen. During the growth process, the flow rate of ammonia was set at 300 sccm and the furnace was maintained at 680 °C for 3 h. Finally, the tube and its contents were rapidly cooled down to room temperature with a cooling rate of 10 °C/min under the protective flow of nitrogen. In order to determine the phase composition of the samples, a powder X-ray diffractometer (Shimadu XRD-6000) with Cu Kα radiation (λ = 1.5418 Å) was used to record the X-ray diffraction (XRD) patterns at a scanning speed of 2 °/min. The accelerating voltage and the applied current were 40 kV and 30 mA, respectively. A HITACHI S4800 field emission scanning electron microscope (FESEM) working at 18.0 kV, which is equipped with an energy dispersive spectrometer (EDS) was used to characterize the size, morphology and composition of the samples. Photoluminescence spectra were examined using a fluorescence spectrophotometer (Edinburgh FLS920) with a Xe lamp excitation at room temperature.

Results and discussion

As shown in Fig. 1a, the diffraction peaks of the products deposited on the Si(100) substrate could be indexed according to the wurtzite InN with the cell parameters a = 3.535 Å, and c = 5.684 Å, which are in good agreement with the values from the standard card (JCPDS No. 50-1239). In addition, the Si (400) peak and SiO_2 (101) peak are all from the substrate. The EDS spectrum also illustrates that the synthesized products consist of only In and N elements (Fig. 1b). The morphology of the prepared InN samples were observed by SEM. As shown in the typical low-magnification SEM image (Fig. 2a,2c), two kinds of microstructures, the microsphere and the split octahedron-like microstructure, were prepared at the upstream (the green area in Fig. 2e) and downstream region (the red area in Fig. 2e) of the Si substrate, separately. The high-magnification SEM image (Fig. 2b) revealed the InN microsphere of ~4-μm diameter contains a rough surface. In combination with the high-magnification SEM images in Fig. S1 (ESI†) and Fig. 2b, it can be clearly observed that the resulting InN spheres are caused by the self-organized of several nanowires. And from different angles of the split octahedron-like microstructure is shown in Fig. 2d, each face of the split octahedron-like microstructure is in regular triangle of a ~1.5 μm-side length.

It is well established that different growth conditions will lead to various morphologies of crystals. In order to reveal the formation process of the InN microstructures in more detail, a series of time-dependent experiments were carried out. And the corresponding XRD analysis and SEM observation were performed to investigate the time-dependent change of the morphology and composition of the samples. Fig. 3 shows XRD patterns of the samples synthesized for 0.5, 1, 1.5, 2, 2.5 and 3 h, respectively. As can be seen from these patterns, at the initial 1 h, these obtained InN subunits showed a extremely low diffraction peak due to the presence of poor crystallized phase. With further increase in the reaction time, XRD patterns

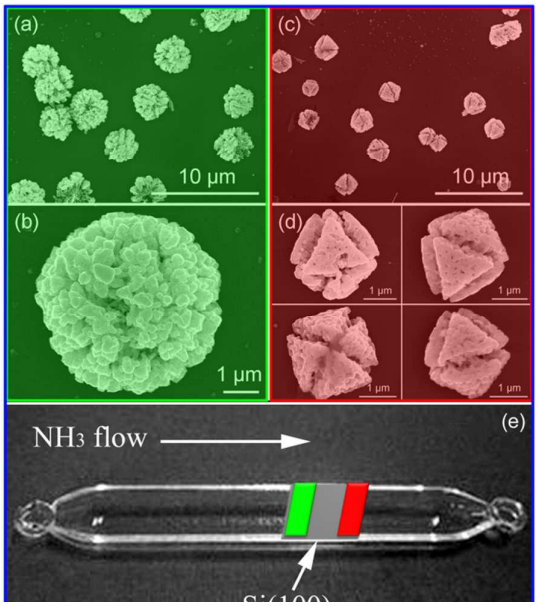

Fig. 2 (a,b) The typical low- and high-magnification SEM images of InN microspheres at the upstream region. (c,d) The typical low- and high-magnification SEM images of the split octahedron-like microstructure at the downstream region. (e) The schematic representation which shown two kinds of InN microstructure were prepared at the upstream and downstream region of the Si substrate separately.

Journal Name

ARTICLE

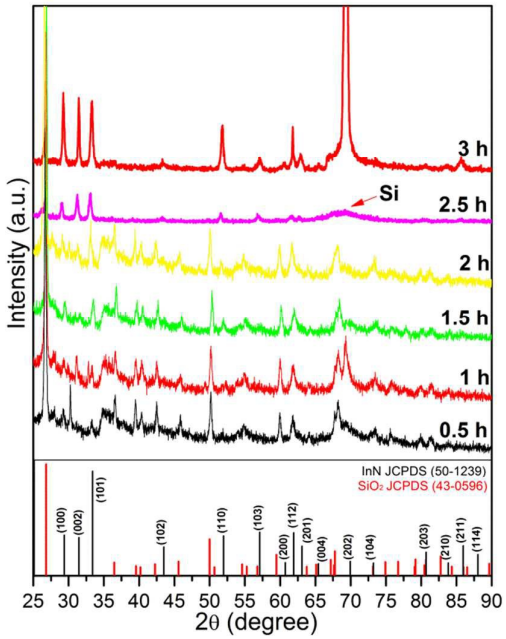

Fig. 3 XRD patterns of products obtained at 680 ℃ for different reaction times.

indicate that the characteristic peak of the InN phase becomes progressively sharper and stronger with longer reaction time. The crystallization of InN was enhanced, as indicated by the higher diffraction intensity. With the reaction time extended to 3 h, The typical XRD patterns of the InN microstructures are illuminated in Fig. 3. All the diffraction peaks are indexed to the wurtzite structure of InN (JCPDS card No. 50-1239) except for the peaks from the Si substrate.

The transformation process of InN was demonstrated in a series of typical SEM images (Fig. 4). A possible schematic representation for the formation of the spherical structure, was described in Fig. 4g. The whole growth process could be divided into four stages. As shown in Fig. 4a, due to the high reaction temperature and NH_3 flow, the nucleation and growth of InN nanowires occurred rapidly in the primary stage (step I).The products composed of nanowires of ~1.5 μm-length were obtained in a short reaction time of 0.5 h. According to Wulff construction, the shape of a crystal is determined by the relative specific energy of crystalline planes.[26,27] As is well known, the growth rate of low-index crystallographic planes is proportional to their surface energies. The fast growing planes with high energy should disappear to leave behind the slowest growing planes with low energy as the exposed facets of the product. Thus, the growth rates of different crystallographic directions are varied and lead to self-organized of low-dimensional products.[28,29] With the elongation of reaction time (step II), for the minimization of the overall energy of the system, several InN nanowires attached by one end until it became brushlike, as shown in Fig. 4b. With the aggregation

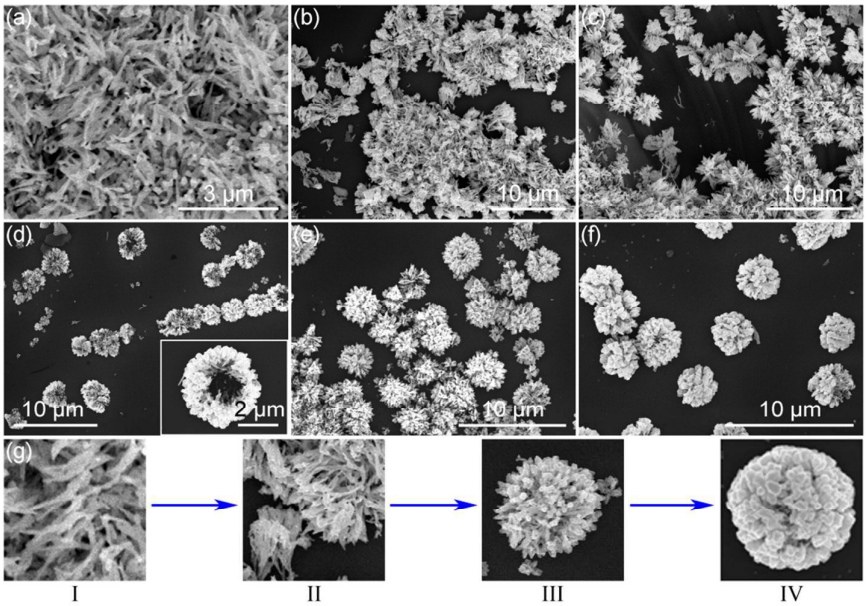

Fig. 4 The SEM images of the InN microspheres formed at different reaction times while all other reaction parameters remain unchanged: (a) 0.5 h, (b) 1 h, (c) 1.5 h, (d) 2 h, (e) 2.5 h, (f) 3h; (g) Schematic illustration for the formation of InN microspheres.

Journal Name

ARTICLE

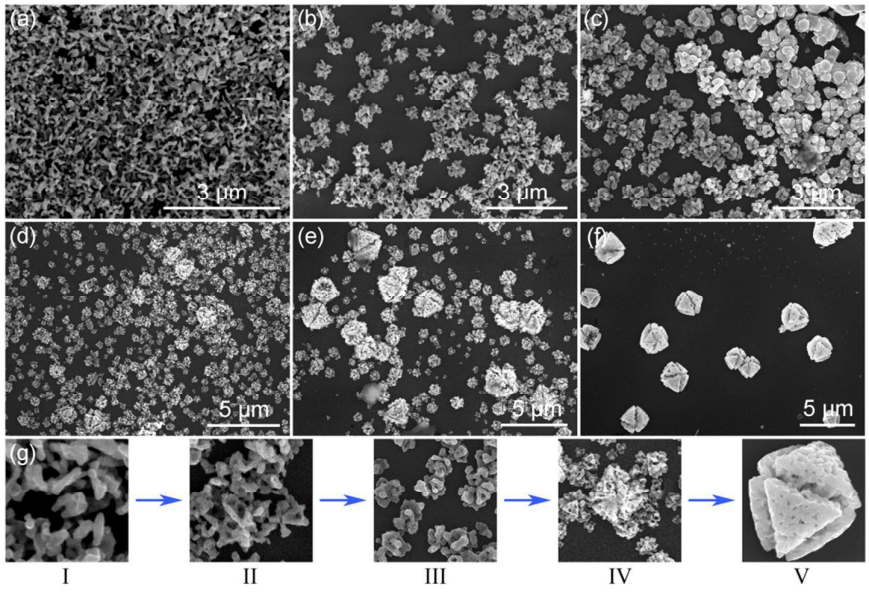

Fig. 5 The SEM images of the split octahedron-like InN microstructure formed at different reaction times while all other reaction parameters remain unchanged: (a) 0.5 h, (b) 1 h, (c) 1.5 h, (d) 2 h, (e) 2.5 h, (f) 3h; (g) Schematic illustration for the formation of split octahedron-like InN microstructures.

process continuing, a large amount of imperfect InN pre-spheres formed at reaction time of 1.5 h (Fig. 4c). As the reaction proceeds, the dispersed nanowires could barely be observed, while the InN microspheres, resulting from the self-organized of nanowires, were further formed (Fig. 4d). When the reaction time is prolonged to 2.5 h (Fig. 4e), as-obtained primary InN microspheres became more complete and the surface of the microsphere became more denser (step III). In this step, these primary InN spheres were metastable due to their high surface energy. In the subsequent crystal growth process (step IV), the reaction rate slowed down due to the depletion of the reactants. Then, in order to reduce the total surface energy, the endpoints of the nanowires at the surface region acted as new nucleation sites. The endpoints grew larger at the expense of reactants.[30] As a result，the surface of the microspheres became more smooth and denser, the regular InN microspheres with rough surface were obtained (Fig. 4f).

The transformation process of the split octahedron-like InN microstructures was also demonstrated in a series of typical SEM images shown in Fig. 5. Instead of the nanowires, the growth process began with the pure InN nanorods with length of around 300 nm (Fig. 5a, step I). As shown in Fig. 5b, after prolonging the reaction time to 1 h (step II), the frames of spiders were constituted by several nanorods and with the elongation of reaction time (step III), aggregated into many irregular micrometer particles to reduce the total surface energy (Fig. 5c). In the subsequent crystal growth process (step IV), the split octahedron-like InN microstructures were taking shape among the micrometer particles after 2 h reaction (Fig. 5d), and then, the less than perfect split octahedron-like InN microstructures were further shaping (Fig. 5e). Similar with the primary InN spheres, the split octahedron-like InN microstructures were metastable due to the high surface energy. Subsequently, in order to further reduce the total surface energy, the defects at the surface region acted as new nucleation sites. At the expense of reactants, the irregular micrometer particles almost disappeared and the surfaces of the spit octahedron-like InN microstructures became flatten gradually. Eventually (step V), the split octahedron-like InN microstructures with smoother surface were obtained (Fig. 5f). And the whole process was also can be clearly shown by simple schematic representation (Fig. 5g). On the basis of the above XRD analysis and SEM observation, the formation of the two InN microstructures could be attributed to the self-organized process, which was also proven in multiple publications for other compounds.[21,30] And the formation of the split octahedron-like InN microstructures is different from the formation of the InN microspheres.

Why is the self-organized process of the two different InN microstructures different?

For the growth of InN micro- or nanostructure via CVD, there are some impacting factors to influence the morphology of the sample. For instance, Naonori Sakamoto et al. reported that the substrate strongly affected crystallization behavior of the InN flowers due to lattice matching between the substrate and InN.[31] Also, the growth temperature has an important effect on morphology of InN materials. InN micro- and nanostructured morphology can be interpreted as a dependence on the degree of supersaturation whereas the morphology of InN 1D nanosturctures can be understood by the kinetics-limited and diffusion-limited processes.[32,33] In addition, NH_3 flux is considered as one of the most impacting parameters in a controlled manner. Liu et al. reported that NH_3 flux had a decisive influence on the growth direction of InN nanowires. Microstructure characterizations of a great number of InN nanowires demonstrated that the growth direction of InN nanowires changes with variable NH_3 flux.[34] In this work, during the growth of InN microstructures, due to the two kinds of microstructures were prepared at different regions of the Si substrate (Fig. 2e). EDS measurements performed on the microspheres and the split octahedron-like microstructures also indicate that the molecular ratio of In : N of the two microstructures was different (Fig. S2, ESI†). We proposed that different self-organized mechanisms could be induced by the difference in nitrogen concentration. To investigate the role of nitrogen concentration in the formation of the InN microstructures, a series of experiments with different flow rate of the ammonia were carried out. On the basis of the SEM observation(Fig. S3, ESI†), it can be concluded that nitrogen concentration has an important effect on morphology of InN microstructures.

As shown in Fig. 6, both the PL spectrum of the InN microspheres and the split aoctahedron-like InN microstructures at room temperature show a similar broad yellow–orange emission band. From the PL spectrum, both the PL emission bands of the InN microspheres and the split octahedron-like InN microstructures centered at ~2.17 eV. This is not similar to the InN microstructures which were report previously.[35] The PL emission bands centered in a range from 0.7 to 2.2 eV have been detected up to now. Yet InN nanostructures show PL emissions at different wavelengths, probably due to existence of the different amounts of defects or surface states.[36,37] It is suggested that the emission centered at 0.7-0.8 eV is the near bandgap emission and the emission centered over 1.7 eV potentially ascribed to the oxygen impurities in InN system, the nitrogen-rich stoichiometry or the Burstein-Moss shift induced by high electron concentrations of the InN microstructures. Yoshimoto et al. reported that oxygen incorporation in InN could result in the wide distribution of band-gap ranging from 1.55 to 2.27 eV, since O contamination leads to larger band-gap energy.[38] However, there is no direct evidence in our study proves that O impurities are introduced into the microstructures, because O impurities cannot be concerned with the whole growth process of InN. It is found that optical absorption edges of InN films and nanowires can range from 0.7 to 1.7 eV due to Burstein-Moss shift.[39] Nevertheless, the experimental conditions indicates that the microstructures appear to be nitrogen rich, nitrogen vacancies are therefore unlikely to be responsible for the commonly observed high background carrier concentration.[40] The band gap of the InN is also found to increase as nitrogen concentration increased.[40,41] The nitrogen defects in the InN microstructures arise from the nucleation and growth of InN subunits, namely, nanowires and nanorods, as well as the self-organized of the subunits.[37,42,43] Compared with other InN nanostructures,[8,37] in our case, the sample grown in a low temperature 680 ℃ as well as the self-organized process would lead to a shorter wavelength emission due to excess nitrogen. We deduce that the nitrogen-rich stoichiometry may be a plausible reason for the ~2.17 eV emission band of the InN microstructures.

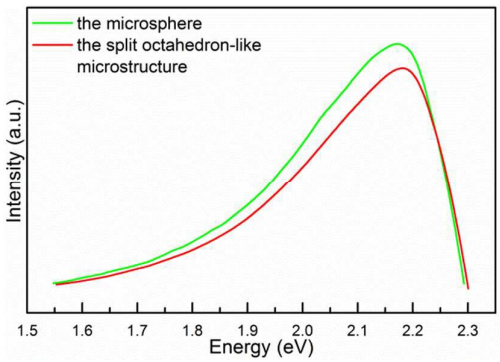

Fig. 6 Room temperature PL spectrum of the InN microspheres and the split octahedron-like InN microstructures at the 510 nm excitation, respectively.

Conclusions

In summary, the InN microspheres and the split octahedron-like InN microstructures were prepared via a simple CVD method without catalyst assisted. The as-synthesized InN microspheres have nearly monodisperse diameters that can be controlled in ~4 μm. And the split octahedron-like InN microstructures are also uniform that the diameters are in the range of 2-3 μm. Detailed study on the growth process suggests different self-organized mechanisms for the growth of the microspheres and the split octahedron-like microstructures. Different organized process leading to different architectures could be induced by the difference in nitrogen concentrations. The nitrogen-rich stoichiometry also play a key role in the ~2.17 eV emission band. The synthesis of the InN microsphere and the split octahedron-like InN microstructure lays foundation for further study on the intrinsic properties of InN nanomaterial and benefits the potential applications in nanodevices and nanosystems.

Acknowledgements

This work was supported in part by the National Natural Science Foundation of China (Grant Nos. 51172087, 11304111, NSAF. No: U1330115), Graduate Innovation Fund of Jilin University (No: 2015140) and Specialized Research Fund for

the Doctoral Program of Higher Education of China (20110061110011) Supported by Graduate Innovation Fund of Jilin University.

Notes and references

1 Z. H. Zhong, F. Qian, D. L. Wang and C. M. Lieber, *Nano lett.*, 2003, **3**, 343.
2 S. X. Li, K. M. Yu, J. Wu, R. E. Jones, W. Walukiewicz, J. W. Ager III, W. Shan, E. E. Haller, H. Lu and W. J. Schaff, *Phys. Rev. B*, 2005, **71**, 161201.
3 R. F. DAVIS, *Proc. IEEE*, 1991, **79**, 702.
4 M. K. I. Senevirathna, S. Gamage, R. Atalay, A. R. Acharya, A. G. U. Perera, N. Dietz, M. Buegler and A. Hoffmann, L. Q. Su, A. Melton, I. Ferguson, *J. Vac. Sci. Technol. A*, 2012, **30**, 031511.
5 F. Qian, M. Brewster, S. K. Lim, Y. Ling, C. Greene, O. Laboutin, J. W. Johnson, S. Gradecak, Y. Cao and Y. Li, *Nano lett.*, 2012, **12**, 3344.
6 J. Wu, W. Walukiewicz, K. M. Yu, J. W. Ager III, E. E. Haller, H. Lu, W. J. Schaff, Y. Saito and Y. Nanishi, *Appl. Phys. Lett.*, 2002, **80**, 3967.
7 K. Sugita, T. Hotta, D. Hironaga, A. Mihara, A. G. Bhuiyan, A. Hashimoto and A. Yamamoto, *Phys. Status Solidi C*, 2012, **9**, 697.
8 T. Matsuoka, H. Okamoto, M. Nakao, H. Harima and E. Kurimoto, *Appl. Phys. Lett.*, 2002, **81**, 1246.
9 Y. Huang, X. F. Duan, Y. Cui and C. M. Lieber, *Nano Lett.*, 2002, **2**, 101.
10 Z. H. Lan, W. M. Wang, C. L. Sun, S. C. Shi, C. W. Hsu, T. T. Chen, K. H. Chen, C. C. Chen, Y. F. Chen and L. C. Chen, *J. Cryst. Growth*, 2004, **269**, 87.
11 E. B. Quddus, A. Wilson, R. A. Webb and G. Koley, *Nanoscale*, 2014, **6**, 1166.
12 M. Lei, K. Huang, R. Zhang, H.J. Yang, X.L. Fu, Y.G. Wang and W.H. Tang, *J. Alloys Compd.*, 2012, **535**, 50.
13 M. S. Hu, G. M. Hsu, K. H. Chen, C. J. Yu, H. C. Hsu, L. C. Chen, J. S. Hwang, L. S. Hong and Y. F. Chen, *Appl. Phys. Lett.*, 2007, **90**, 123109.
14 M. H. Kim, D. Y. Moon, J. Park, Y. Nanishi, G. C. Yi and E. Yoon, *Phys. Status Solidi A*, 2012, **209**, 50.
15 Y. L. Chang, F. Li, A. Fatehi and Z. Mi, *Nanotechnology*, 2009, **20**, 345203
16 S. D. Luo, W. Y. Zhou, Z. X. Zhang, L. F. Liu, X. Y. Dou, J. X. Wang,X. W. Zhao, D. F. Liu, Y. Gao, L. Song, Y. J. Xiang, J. J. Zhou and S. S. Xie, *Small*, 2005, **1**, 1004.
17 S. H. Yun, Y. H. Ra, Y. M. Lee, K. Y. Song, J. H. Cha, H. C. Lim, D. W. Kim, N. J. S. Kissinger and C. R. Lee, *J. Cryst. Growth* 2010, **312**, 2201.
18 M. A. Sánchez-García, J. Grandal, E. Callejal, S. Lazic, J. M. Calleja and A. Trampert, *Phys. Status Solidi B*, 2006, **243**, 1490.
19 C. K. Chao, J. I. Chyi, C. N. Hsiao, C. C. Kei, S. Y. Kuo, H. S. Chang and T. M. Hsu, *Appl. Phys. Lett.*, 2006, **88**, 233111.
20 N. Nepal, N. A. Mahadik, L. O. Nyakiti, S. B. Qadri, M. J. Mehl, J. K. Hite, C. R. Eddy, *Cryst. Growth Des.*, 2013, **13**, 1485.
21 M. Li, H. Schnablegger and S. Mann, Nature, 1999, **402**, 393.
22 G. C. Xi, C. Wang and X. Wang, *Eur. J. Inorg. Chem.*, 2008, **3**, 425.
23 Q. Peng, S. Xu, Z. B. Zhuang, X. Wang, and Y. D. Li, *small* 2005, **1**, 216.
24 S. X. Tang, H. Y. Zhu, J. R. Jiang, X. X. Wu, Y. X. Dong, J. Zhang, D. P. Yang , Q. L. Cui, *Chin. Phys. B*, 2015, **24**, 096101.
25 H. Y. Xu, Z. Liu, X. T. Zhang and S. K. Hark, *Appl. Phys. Lett.*, 2007, **90**, 3105.
26 Z. L. Wang, *J. Phys. Chem. B*, 2000, **104**, 1153.
27 S. X. Tang, J. Zhang, S. Wu, C. Y. Hu, Y. A. Li, L. N. Jiang and Q. L. Cui, *J. Phys. Chem. C*, 2014, **118**, 21170.
28 L. W. Qian, J. Zhu, Z. Chen, Y. C. Gui, Q. Gong, Y. P. Yuan, J. T. Zai, and X. F. Qian, *Chem. Eur. J.* 2009, **15**, 1233.
29 S. Wu, J. Zhang, L. H. Shi, S. X. Tang, Y. A. Li, L. N. Jiang and Q. L. Cui, *RSC Adv.*, 2014, **4**, 8209.
30 X. M. Yin, C. C. Li, M. Zhang, Q. Y. Hao, S. Liu, L. B. Chen and T. H. Wang, *J. Phys. Chem. C*, 2010, **114**, 8084.
31 N. Sakamoto, H. Sugiura, D. Fu, N Wakiya and H. Suzuki, *Key Eng. Mater.*, 2010, **445**, 209.
32 F. Zhang, Q. Wu, Y. L. Zhang, J. M. Zhu, N. Liu, J. Yang, X. Z. Wang and Z. Hu, *Appl. Surf. Sci.*, 2012, **258**, 9701.
33 Y. N. Xia, P. D. Yang, Y. G. Sun, Y. Y. Wu, B. Mayers, B. Gates, Y. D. Yin, F. Kim and H. Q. Yan, *Adv. Mater.*, 2003, **15**, 353.
34 H. Liu, L. Shi, X. Geng, R. Su, G. Cheng and S. Xie, *Nanotechnology*, 2010, **21**, 245601.
35 C. H. Liang, L. C. Chen, J. S. Hwang, K. H. Chen, Y. T. Hung and Y. F. Chen, *Appl. Phys. Lett.*, 2002, **81**, 22.
36 S. Kolli, C. S. Pendyala, M. Sunkara, J. Jasinski and B. Alphenaar, *J. Lumin.*, 2013, **141**, 162.
37 J. Zhang, B. Xu, F. Jiang, Y. Yang and J. Li, *Phys. Lett. A*, 2005, **337**, 121.
38 M. Yoshimoto, H. Yamamoto, W. Huang, H. Harima, J. Saraie, A. Chayahara and Y. Horino, *Appl. Phys. Lett.*, 2003, **83**, 3480.
39 V. Y. Davydov, A. A. Klochikhin, V. V. Emtsev, S. V. Ivanov, V. V. Vekshin, F. Bechstedt, J. Furthmüller, H. Harima, A. V. Mudryi, A. Hashimoto, A. Yamamoto, J. Aderhold, J. Graul, and E. E. Haller, *Phys. Status Solidi B*, 2002, **230**, R4.
40 K. S. A. Butcher, M. Wintrebert-Fouquet, P. P. T. Chen, T. L. Tansley, H. Dou, S. K. Shrestha, H. Timmers, M. Kuball, K. E. Prince and J. E. Bradby, *J. Appl. Phys.*, 2004, **95**, 6124.
41 K. Scott, A. Butcher, M. Wintrebert-Fouquet, P. P. T. Chen, K. E. Prince, H. Timmers, S. K. Shrestha, T. V. Shubina, S. V. Ivanov, R. Wuhrer, M. R. Phillips and B. Monemar, *Phys. Status Solidi C*, 2005, **2**, 2263.
42 T. Tang, S. Han, W. Jin, X. Liu, C. Li, D. Zhang, C. Zhou, B. Chen, J. Han and M. Meyyapan, *J. Mater. Res.*, 2004, **19(02)**, 423.
43 H. H. Jiang, L. C. Zhao, L. G. Gai, L. Ma, Y. Ma and M. Li *CrystEngComm*, 2013, **15**, 7003

TOC: Two kinds of 3D InN microstructures were prepared via the different self-organized processes at the up- and down-stream regions of the Si substrate.